A Single-Port Robotic System for Transanal Micro-Surgery – Design and Validation

Jianzhong Shang[1], Konrad Leibrandt[1], Petros Giataganas[1], Valentina Vitiello[1], Carlo A. Seneci[1], Piyamate Wisanuvej[1,2], Jindong Liu[1], Gauthier Gras[1], James Clark[1,3], Ara Darzi[1,4] and Guang-Zhong Yang[1], *Fellow, IEEE*

***Abstract*—This paper introduces a single-port robotic platform for Transanal Endoscopic Micro-Surgery (TEMS). Two robotically controlled articulated surgical instruments are inserted via a transanal approach to perform submucosal or full-thickness dissection. This system is intended to replace the conventional TEMS approach that uses manual laparoscopic instruments. The new system is based on master-slave robotically controlled tele-manipulation. The slave robot comprises a support arm that is mounted on the operating table, supporting a surgical port and a robotic platform that drives the surgical instruments. The master console includes a pair of haptic devices, as well as a 3D display showing the live video stream of a stereo endoscope inserted through the surgical port. The surgical instrumentation consists of energy delivery devices, graspers and needle drivers allowing a full TEMS procedure to be performed. Results from benchtop tests, *ex-vivo* animal tissue evaluation and *in-vivo* studies demonstrate the clinical advantage of the proposed system.**

***Index Terms*—Robotic Surgery, Single-Port Surgery, Surgical Robotics, Transanal Endoscopic MicroSurgery**

I. Introduction

Colorectal cancer is the third most commonly diagnosed malignancy worldwide and the fourth leading cause of cancer death in the world [1]. Currently, one third of the cancerous lesions identified tend to be early stage tumours and are, in those accessible, suitable for local transanal excision over conventional open surgery without compromise of oncological treatment. Transanal Endoscopic Micro-surgery (TEMS) is a well developed technique for the safe and effective excision of early stage tumours and high grade adenomas; the benign precursors to malignancy, within the rectum and recto-sigmoid. The approach is in essence a single-port laparoscopic technique. However, operating within a narrow space through a single-port using rigid pre-bent laparoscopic instruments, as is the case with the TEMS approach, is highly challenging and limits the potential of the technique. Many of the challenges with this single-port technique are ergonomic in nature and well described. Of particular note is the limited external workspace available to the operator, restricting their ability to triangulate the instruments and perform dexterous manipulation. Other limitations include the fulcrum effect, which describes the inversion of the instrument's movements relative to the surgeon's hand motion. In addition, the tool leverage that occurs within the port can lead to the inaccurate representation of forces applied to the tissue. A robotic system can overcome these problems and enable the possibilities of TEMS and transanal procedures in general to broaden beyond the current constraints, with the potential to treat even more patients with the condition in a minimally invasive way, more effectively and potentially with lower risk.

While single-port access surgery has been explored extensively the only robotic platform for single-port surgery currently on the market is the da Vinci® Single-Site® (Intuitive Surgical Inc., Sunnyvale, CA) [2]. It features two semi-rigid instruments inserted through two curved cannulae crossing each other at the port entry point to provide triangulation. This configuration is however not suitable for surgeries within a confined space. A number of other single-port robotic platforms are currently under development. The da Vinci® SP™ system [3], also by Intuitive Surgical Inc., incorporates three 6mm, 7 Degrees-of-Freedom (DoFs) surgical tools and a stereo camera inserted through a single-port. All the instruments and camera are straight during insertion to fit in the 25mm surgical port. Once the instruments and camera are inserted, they can be reconfigured to provide off-axis camera view and instrument triangulation. The da Vinci® SP™ system received FDA 510(k) clearance in 2014 initially for urological procedures that are suitable for single-port surgery and is expected to be available on the market soon. Similarly, the single-port surgical system developed by Samsung Electronics [4] features a 6-DoF guide tube, two 7-DoF surgical tools, and a 3-DoF stereo-endoscope. The 30mm diameter guide tube consists of two 2-DoF segments with variable stiffness rolling joints and has sufficient flexibility to reach a surgical target in an arbitrary pose within the abdomen. The multi-DoF instruments can cover 250mm(W) x 200mm(H) x 200mm(D) space. The SPORT™ (Single Port Orifice Robotic Technology) Surgical System (Titan Medical Inc. Toronto, Canada) is based on the IREP system [5] that has two multi-DoF continuum arms and a 3-DoF stereo camera. The system can pass through a 15mm port and covers a large workspace of 64mm x 103mm. The SurgiBot™ by TransEnterix Inc. (Morrisville, NC) is another single-port access robot based on the manual SPIDER® system [6]. Studies on simulators presented that to use the SPIDER® system is more challenging compared to the conventional multiport laparoscopic surgery approach [7]. The robotic version of this system is set to improve the shortcomings of the manual system. However, since the rejection of the initial FDA 510(k) clearance application in 2015, the system is not expected to be on the market in the near future. Researchers from Waseda University, Japan, developed a

Manuscript received: *September 11, 2016*; Revised *December 16, 2016*; Accepted *January 24, 2017*.

This paper was recommended for publication by Editor *Ken Masamune* upon evaluation of the Associate Editor and Reviewers' comments. This work is supported by the Wellcome Trust and the Department of Health through the Health Innovation Challenge Fund (HICF-T4-299).

[1]All authors are with the Hamlyn Centre, Imperial College London. [2]Piyamate Wisanuvej is also with Kasetsart University, Bankok, Thailand. [3]James Clark is also a General Surgical Registrar ST8 at Southwest Peninsula Deanery. [4]A. Darzi is also with the Department of Surgery and Cancer, Imperial College London, London, United Kingdom. Corresponding author: Jianzhong Shang (e-mail: j.shang@imperial.ac.uk).

Digital Object Identifier (DOI): See top of this page.

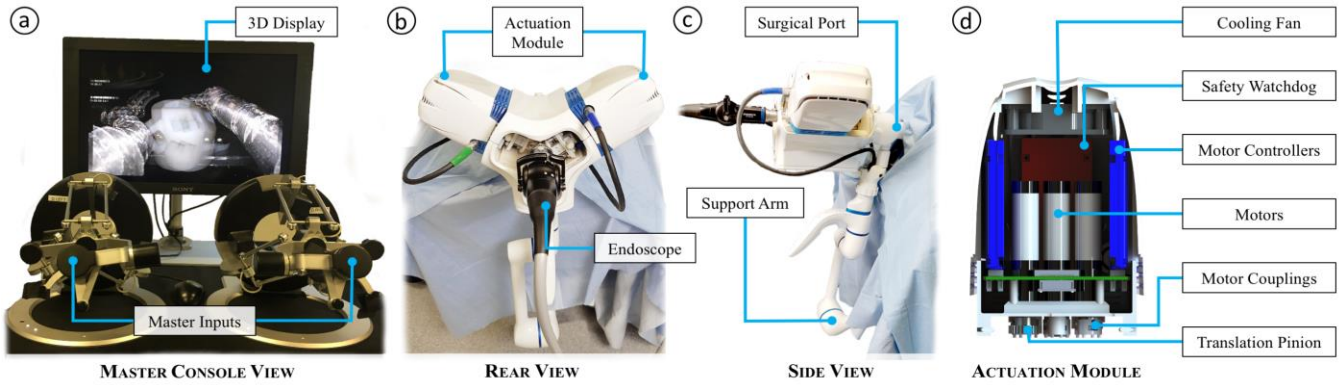

Fig. 1. Main components of the micro-IGES system, presenting (a) the master console, (b) the actuation modules and endoscope, (c) the surgical port and supporting arm, and (d) the internal components of the actuation module.

master-slave single-port surgical robot that has a 25mm flexible shaft, two 8mm 6-DoF instruments, and a camera that can be manipulated to adjust the field of view [8]. In previous work, the authors reported a multitasking robotic platform for single-port access surgery in [9]. This system incorporates two continuum arms with surgical instruments and a 3-DoF "head" for manipulating the camera and an additional instrument. A common drawback of all these systems is that they are mainly designed for operation within the abdominal cavity. The configuration of the camera and the size of the instruments therefore prevents their deployment within such a narrow and confined space as the rectum.

A number of devices targeting flexible access applications for Natural Orifice Transluminal Endoscopic Surgery (NOTES) have surgical instruments integrated at the front of flexible endoscopes, such as the ANUBISCOPE® (iCUBE STRAS) robot developed at IRCAD-Strasbourg, that is based on the Karl Storz® Anubis® system, the R-scope and Endo-Samurai by Olympus. A review of such flexible access NOTES systems can be found in [10]. Although promising, these systems still lack of adequate stability, triangulation and force exertion capabilities to carry out complex tissue manipulation, as required during TEMS.

This work presents a novel robotic platform, entitled as "micro-IGES robotic system", which is suitable for performing complex surgical tasks in a confined workspace, while improving the precision of operation and the ergonomics for the surgeon. In addition, the robot is light-weight and has a small footprint in operating room. An overview of the robotic system design is given in section II. The robot control and system integration are described in section III, followed by experimental results of the system validation in section IV. Section V concludes the paper.

II. Robotic System Design

A. Overview of the Robotic System

The micro-IGES robotic system aims to create a unique operating experience for the end user and ultimately a better outcome for the patient through its ability to overcome the many ergonomic challenges of conventional single-port surgery. It aims to deliver a lightweight (3 kg), compact and transportable master-slave bimanual system (Fig. 1). The slave system has a footprint of 0.35m(W) x 0.5m(H) x 0.5m(D) and the instruments are designed for operation in confined surgical environments, such as those encountered in transanal excisions of rectal lesions.

The system includes a master console as shown in Fig. 1 (a), which consists of a pair of omega.7 haptic devices (Force Dimension, Nyon, Switzerland), a foot-pedal, a 3D display and a control computer. The slave robot consists of a support arm attached to the operating table using universal fittings enabling full support at all times but with a simple re-positioning system for controlled smooth re-adjustments, a port that is inserted into the patient, two multi-DoF surgical instruments with actuation pack units, and a 3D stereo camera for visualisation. Each of the main components is described in details in the following section.

B. Main Components of the System

1) Support Arm

The whole slave robot platform is supported by the Hamlyn Lightweight Robot Arm® directly mounted on the surgical bed, as shown in Fig. 1 (b-c). The support arm is an articulated passive arm with six revolute joints and 5 kg payload. Each joint has an electro-magnetic brake to lock the arm in position. The brakes are released when powered on, and locked when powered off. This feature ensures the arm is safe in case of an accidental power cut. A handle with two buttons, one on the top and the other one on the bottom, is used to activate the arm. The arm can be manipulated only when both buttons are pressed. The surgical port together with the robotic platform are mounted on the end of the support arm, so that their position can be adjusted by manipulating the arm. Once the port is moved to a suitable position, the arm is locked and the robotic platform is rendered rigid and secure for the operation. Additionally, all power and electrical cables linking the master and slave devices are all fed through and embedded within the arm to minimise cable clutter and maximise the safety of the working environment.

Furthermore, the arm also incorporates an absolute encoder in each joint. This enables global positioning of the instrument base to achieve accurate co-registration for intra-operative image guidance, as well as force estimations at the surgical port based on encoder values, using a method similar to [11].

2) Surgical Port

The micro-IGES surgical port is 36mm in diameter and offered in various lengths to enable access to lesions at different depth within the rectum. The currently marketed conventional TEMS ports including the TEO® Operating Rectoscope Tube

This article has been accepted for publication in a future issue of this journal, but has not been fully edited. Content may change prior to final publication. Citation information: DOI 10.1109/LRA.2017.2668461, IEEE Robotics and Automation Letters

(Karl Storz GmbH, Germany), and the TEM operating proctoscope (Richard-Wolf GmbH, Germany) work within a diameter of 40mm due to the limited instrument triangulation achieved at smaller sizes. Minimising the port size minimises any potential injury to the patient's muscles of continence. The micro-IGES port is compatible with both the robotic system and the conventional instrumentation, ensuring patient safety is not compromised in the unlikely event of system failure.

The micro-IGES surgical port features four valves, two on the horizontal plane to allow the left and right surgical instruments to access the surgical site, one at the top for the camera and one at the bottom for auxiliary. The port also features a camera fixation knob, an insufflation air inlet and release connectors and interface to the actuation pack. The port is fabricated with fused deposition modelling prototyping process with ABS M30i thermoplastic material (Fortus 400mc, Stratasys Ltd., USA) that is biocompatible and can be sterilised using Ethylene Oxide process for clinical use.

3) Actuation Pack

The actuation pack consists of a linear rail and two motor packs that drive the two instruments.

The linear rail is attached to the port with a quick locking mechanism and supported by the support arm for enhanced stability. Each motor pack accommodates seven brushless direct current motors (BLDC, Maxon EC13) with factory assembled encoders (MR Type L, 256 counts per turn) and gearheads (67:1). Although the driving force for different instrument joints varies, same motors are chosen to drive all the joints to simplify the design and motor control. The motors are all arranged in parallel to save space, as shown in Fig. 1(d). The control electronics include four custom-made motor control modules and a custom-made safety watchdog module plugged onto a motherboard that is designed to hold all the control modules arranged around the motors. Each motor control module can drive two motors. Since all seven motors and their controllers are packed in a small space, heat dissipation is of great importance. An axial DC cooling fan is mounted at the top of the motor pack. Careful consideration was taken to ensure the airflow goes through the motors and motor controllers and exits from the top. Six out of the seven motors have spring loaded motor couplings that interface with the respective instrument to drive the six DoFs built into the instrument. The seventh motor has a pinion attached that meshes with a rack that is fixed on the linear rail for linear translation.

4) Articulated Instruments

A number of instruments have been designed for different tasks. A typical instrument features a maximum of 7-DoFs as presented in Fig. 2. These include end-effector open/close, 2-DoF wrist (yaw and pitch), 2-DoF flexible elbow (yaw and pitch) and a rigid shaft that rotates about its axis (roll). The rigid shaft connects the articulated instrument tip to the driving unit. The seventh-DoF translates the whole instrument (translation).

The end-effector is composed of nine segments that are produced with selective laser melting, following the findings presented in [12]. The components are polished after the 3D printing process. Each of the articulation joints is driven by an antagonistic pair of tendons made of 7x19 strand stainless steel 304V. The tendon is 0.45mm in diameter with a tensile strength of 110N. Tendons are fixated to their linkages by stamping to avoid the use of additional termination elements such as ferrules,

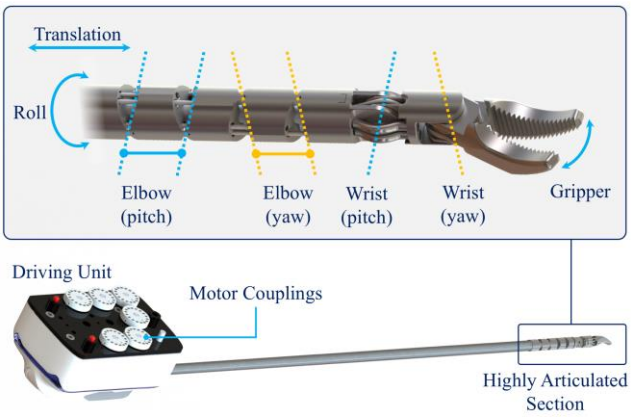

Fig. 2. Instrument articulated tip and driving unit.

therefore providing a more compact solution, ideal for miniaturised instruments. The flexible elbow has two segments moving on perpendicular planes, each featuring two serially linked joints. The two joints in the same plane are mechanically coupled to travel at the same angle thanks to a coupling mechanism that uses spur gears to couple the motion between the capstans that drive the tendons. Two serially linked joints travelling in the same plane increases the joint travel range without experiencing sharp bends, compared to only one joint travelling to the same angle. The most demanding joint to deliver lateral force is the one at the proximal end of the elbow, where the cantilever distance is the longest at 19mm. With an offset from the tendon to the joint axis of 2mm, the lateral force delivered to the instrument tip specified to be 5N, the maximum tendon tension is calculated to be 65N. In practice, the motor output is limited to avoid damage and the maximum lateral force measured at the instrument tip is 3.5N.

The three pairs of tendons that drive the wristed end-effector are routed through a multi-lumen Polytetrafluoroethylene (PTFE) catheter that passes through the central channel of the flexible elbow. This arrangement minimises the crosstalk that can affect the end-effector performance when the flexible elbow is actuated. All the tendons that drive the articulated joints are passed through the rigid shaft to the driving unit at the proximal end of the instrument. Each tendon pair goes through a series of pulleys located at the driving unit to find its corresponding driving capstan. The two capstans that drive the two serial joint links bending in the same plane of each flexible elbow segment are coupled by a series of gears with 1:2 ratio. This ensures that the same bending angle is achieved for the two joints, as the tendon that drives the joint further away from the driving unit travels twice as much as the tendon that drives the joint closer to the driving unit. The shaft is driven in the same fashion with an antagonistic pair of tendons wrapped around the shaft and routed to the capstan located at the driving unit. The capstans are all arranged in the same direction with couplings attached to the capstan shafts for motor interfacing.

The instrument shaft is 5mm in diameter and 250mm in length. The travel range of each elbow joint is +/-45°. The travel range for the wrist joints is +/-90°, while the jaws can open as wide as 180°. The instrument rotates about the rigid shaft by +/-180° and translation range is 80mm. The workspace coverage is shown in Fig. 3. With the capability of repositioning the robot by manipulating the support arm, and various lengths of the surgical port, the workspace is sufficient to cover the entire

rectum that typically has 40mm diameter and extends up to 200mm in depth from the anus [13].

III. Instrument Control and System Integration

A. Instrument Control Interface

Users can interact with the system via a pair of haptic devices (for bimanual manipulation) as well as a foot-pedal, as shown in Fig. 4. The system uses a high-level control interface to generate the desired robot response based on the user inputs. In particular, the instrument control interface provides four different functions: mapping of the inputs from the bimanual haptic interface to the workspace of each tool, scaling, clutching and enforcing workspace boundary restrictions.

In order to offer fine control of the instrument motion, the commanded end-effector translation, rotation, and gripper strength can be scaled as desired. While orientation scaling can be useful in specific situations where very fine wrist motions are needed, it is typically best to disable it in order to retain an intuitive mapping between the hand orientation and the instrument orientation. Clutching of the instruments is also implemented to allow the user to reposition the haptic devices when they reach the end of their workspace. As with scaling, clutching of the orientation is possible but not recommended in order to keep an intuitive mapping between the hand and the tool. Lastly, a boundary restriction is implemented to prevent the end-effector set-point from moving too far outside the instrument workspace. This is achieved by constraining the set-point generated by the haptic devices to be within a specific volume. This volume is obtained from a workspace analysis of the instrument, in order to limit the risk of the user commanding the tool to move outside of its reachable workspace. Fig. 3. shows the left instrument workspace in green, the right instrument workspace in blue and the intersecting workspace in yellow.

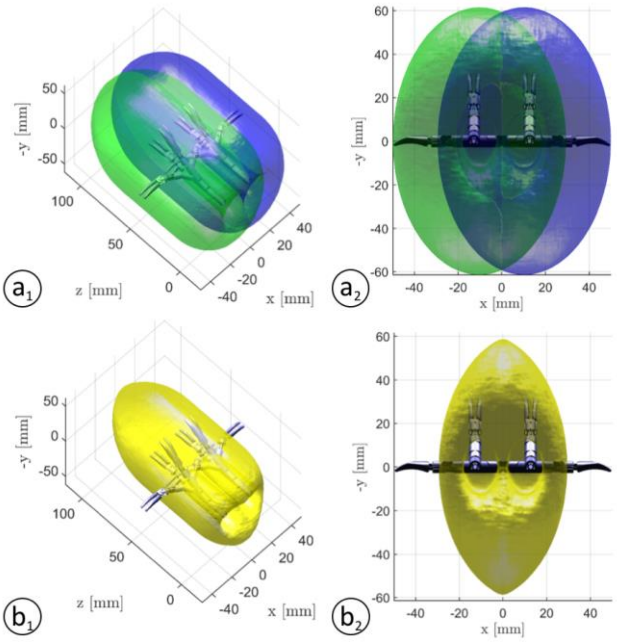

Fig. 3. (a) The left instrument workspace is displayed in green and the right instrument workspace is displayed in blue. (b) The instruments' intersecting workspace is shown in yellow. Cross-sectional views are displayed on the right.

B. Kinematic Control

The inverse kinematics of the tools is based on the local kinematics using the Jacobian, which relates joint space velocities to task space velocities ($\dot{\boldsymbol{x}} = \boldsymbol{J}\dot{\boldsymbol{q}}$). A particular emphasis is laid on avoiding joint limits and dealing with configurations in joint limits. The task space $\boldsymbol{x} = [t_x, t_y, t_z, r_x, r_y, r_z]^T$ is divided into primary $\boldsymbol{x}_p = [t_x, t_y, t_z, r_z]^T$ (translations and roll), and secondary $\boldsymbol{x}_s = [r_x, r_y]^T$ (pitch, and yaw) goals. Using the damped-least-square (DLS) inverse Jacobian ($\boldsymbol{J}^\star$):

$$\boldsymbol{J}^\star = \boldsymbol{V}\,\mathrm{diag}\left(\frac{\sigma_1}{{\sigma_1}^2+\lambda^2}, \cdots, \frac{\sigma_n}{{\sigma_n}^2+\lambda^2}\right)\boldsymbol{U}^T \tag{1}$$

with ${\sigma_i}^2$ the Jacobian's eigenvalues, and $\boldsymbol{V}$, $\boldsymbol{U}$ the right and left singular vectors, all obtained from a singular value decomposition (SVD), and the λ-parameter controlling the damping, to avoid high joint velocities when close to singularities. Furthermore, to avoid joint limits the DLS inverse Jacobian for the primary ($\boldsymbol{J}_p^\star$) and secondary ($\boldsymbol{J}_s^\star$) task space goals are calculated using (1) to perform a joint update using:

$$\boldsymbol{q}_t = \boldsymbol{q}_{t-1} + \Delta\boldsymbol{q}_t = \boldsymbol{q}_{t-1} + \dot{\boldsymbol{q}}_{t-1}\Delta t, \tag{2}$$

$$\dot{\boldsymbol{q}}_{t-1} = \boldsymbol{J}_p^\star\,\boldsymbol{x}_p + \left(\boldsymbol{I_6} - \boldsymbol{J}_p^\star\boldsymbol{J_p}\right)\dot{\boldsymbol{q}}_{null}, \tag{3}$$

$$\dot{\boldsymbol{q}}_{null} = \boldsymbol{f}_{\mathrm{ori}}\left(\dot{\boldsymbol{x}}_{\boldsymbol{p}}, \dot{\boldsymbol{x}}_{\boldsymbol{s}}, \boldsymbol{J}_s^\star\right) + \boldsymbol{f}_{\mathrm{lim}}(\boldsymbol{q}_{t-1}). \tag{4}$$

The secondary goal objective function in (4) $\boldsymbol{f}_{\mathrm{ori}}$ optimises user specified tool orientation in pitch and yaw, and $\boldsymbol{f}_{\mathrm{lim}}$ optimises the avoidance of joint limits. They are defined as:

$$\boldsymbol{f}_{\mathrm{ori}} = k_{ori}\left(1 - \frac{\min(\|\dot{\boldsymbol{x}}_p\|, \dot{x}_{p,\max})}{\dot{x}_{p,\max}}\right)\boldsymbol{J}_s^\star\,\dot{\boldsymbol{x}}_{\boldsymbol{s}} \tag{5}$$

for the secondary orientations and as:

$$f_{\mathrm{qlim},i} = k_{\mathrm{qlim}}\left|\frac{q_{i,\max} + q_{i,\min} - 2q_i}{q_{i,\max} - q_{i,\min}}\right|^{k_e} \cdot \mathrm{sgn}\left(q_i - \frac{q_{i,\max}+q_{i,\min}}{2}\right), \tag{6}$$

for the joint limits, where the exponent k_e (here set to 3) scales the cost function such that the joint limit optimisation is mainly active close to the limit. More detailed kinematic analysis and tool calibration of this system can be found in [14].

C. System Integration and Safety Considerations

Fig. 4 shows the control architecture of the robot system. The master control console includes a pair of omega.7 haptic devices and a foot-pedal as input devices, and a 3D screen displaying the camera view is used as feedback to the operator. The movements of the haptic device handles are mapped to the two instruments respectively. One key on the foot-pedal is used to activate/ deactivate the control output, and the other to clutch the haptic devices to increase the effective travel range.

Bidirectional communication between the control computer and the motor controllers is implemented on an RS485 bus. Commands from the computer are delivered to the left and right motor packs via a Y split cable. Additionally, safety watchdog modules also monitor this communication bus to detect erroneous messages and act accordingly. The safety watchdog modules also communicate with the computer via a dedicated RS485 channel for system startup, diagnostic, and fault recovery purposes.

This article has been accepted for publication in a future issue of this journal, but has not been fully edited. Content may change prior to final publication. Citation information: DOI 10.1109/LRA.2017.2668461, IEEE Robotics and Automation Letters

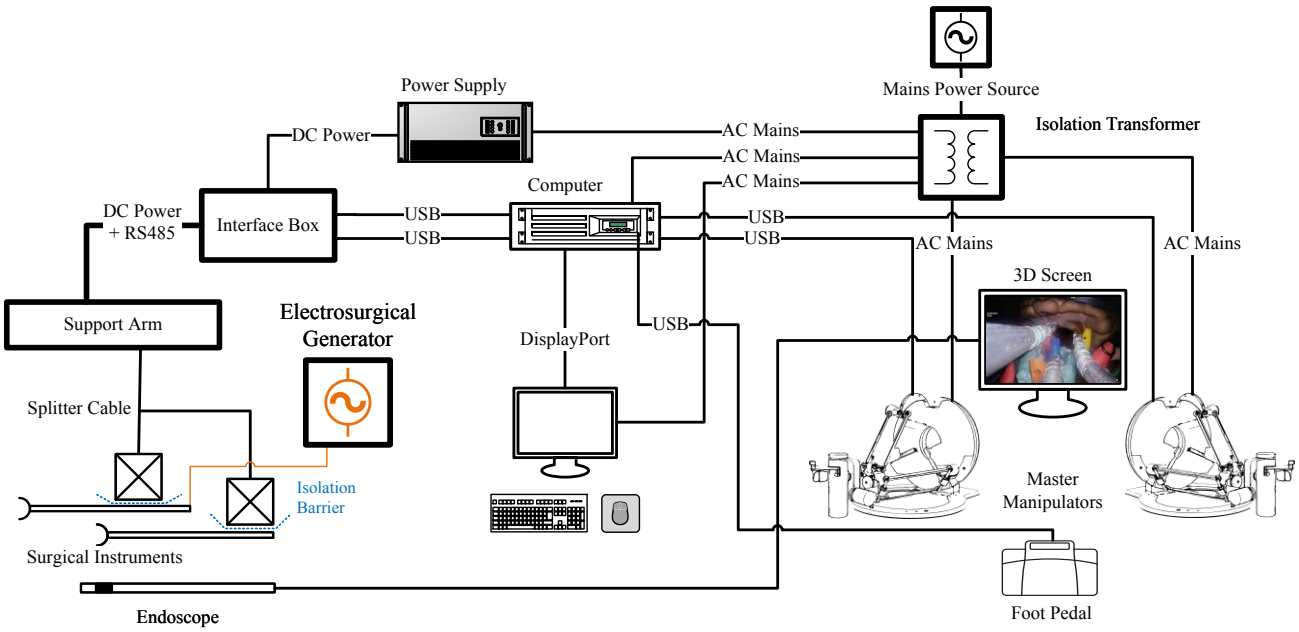

Fig. 4. Control system architecture presenting communication and power lines of the complete robotic system.

All the motor control modules are identical, and so are all the safety watchdog modules. The benefit of this feature is that any module can easily be replaced with a new one in the case of malfunction. This is achievable by integrating the control module address identification into the motherboard circuit. This identifies the address of each socket accommodating a control module.

All the motors have safety margins regarding motor current, velocity and position, which are enforced when driving the instruments. On one hand, the current limit cannot be too low in order to ensure sufficient torques are delivered to the instrument joints when performing tasks demanding high forces, *e.g.* suturing, or tissue manipulation. On the other hand, it can be potentially dangerous when excessive forces are exerted onto delicate tissue. Therefore, safety margins were carefully calibrated so that the required maneuvers in TEMS can be performed while excessive forces on tissue and instrument components are avoided.

When cauterisation is needed, electrical power generated by a diathermy device is delivered to the instrument tip through the shaft. The electrical current has the potential to damage the drive electronics of both instruments, as they are electrically coupled via the tissue. Therefore, to avoid a system failure, all motor couplings are made of polyether ether ketone (PEEK) to electrically isolate the driving unit from the instruments.

IV. User Trials and *In-Vivo* Results

In general, TEMS involves three distinct surgical task requirements: identification and marking of the lesion to be excised, excision of the lesion and wound closure. The marking is performed using electrocautery creating dot burns circumferentially around the lesion. The lesion is then excised in a "join the dots" fashion before the remaining defect is closed using a running suture and knot tie. Trials were designed and performed to test the specific ergonomic limits and dexterity of the robotic system as well as the clinical relevance for this targeted transanal application. These included a series of benchtop and *ex-vivo* tissue trials as well as an *in-vivo* animal trial.

A. Benchtop Trials

1) Lesion targeting and marking

The aim of the first user trial was to assess the accuracy of instrument positioning at different locations within the rectum workspace, by mimicking a lesion marking task. Five engineer users were asked to perform a targeting task by placing the distal tip of the instrument on eight distinct points along a circle.

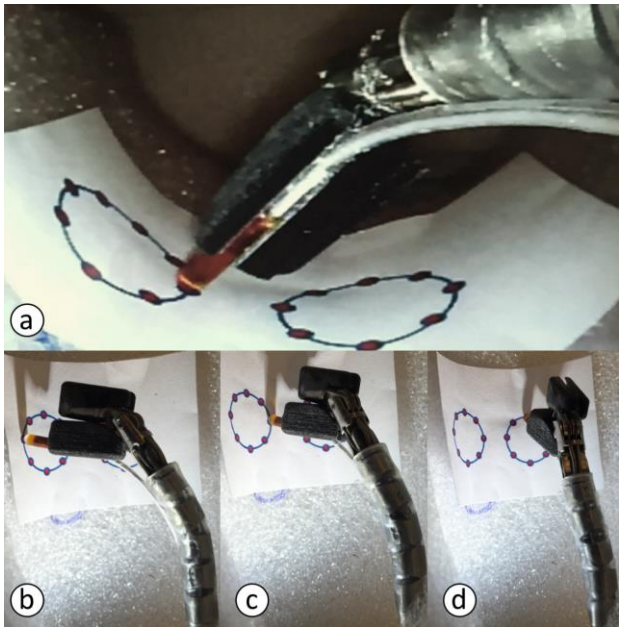

Fig. 5. Example snapshots of the targeting task user trials. a) Camera view of the instrument with electromagnetic probe mounted at the tip. b-d) Top view of the instrument at three different target locations.

This article has been accepted for publication in a future issue of this journal, but has not been fully edited. Content may change prior to final publication. Citation information: DOI 10.1109/LRA.2017.2668461, IEEE Robotics and Automation Letters

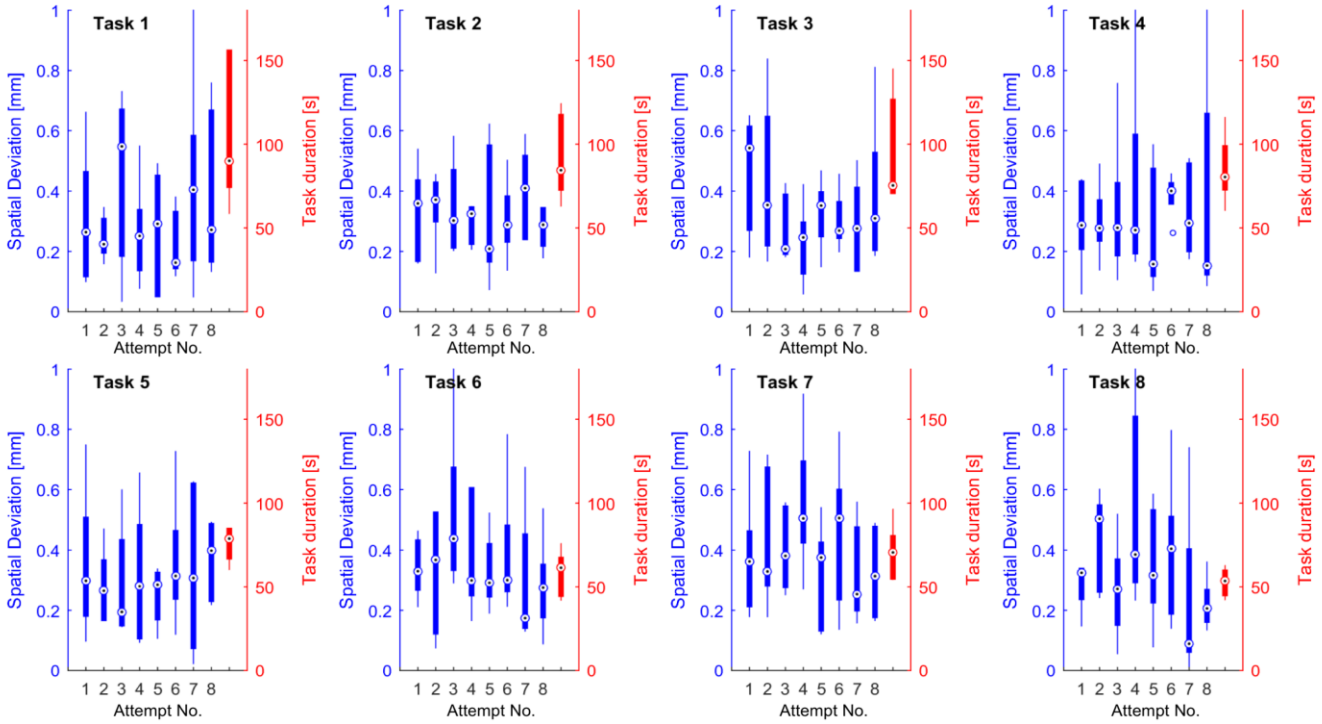

Fig. 6. Results of the targeting task user trials. Task 1: small circle at 0° and scaling factor of 0.3; Task 2: small circle at 0° and scaling factor of 0.1; Task 3: small circle at 45° and scaling factor of 0.3; Task 4: small circle at 45° and scaling factor of 0.1; Task 5: big circle at 0° using a non-wristed instrument; Task 6: big circle at 45° using a non-wristed instrument; Task 7: big circle at 0° using a wristed instrument; Task 8: big circle at 45° using a wristed instrument.

The circle was placed within a plastic cylindrical tube to represent a lesion on the rectal wall. The task was performed using two circle diameters (12mm and 20mm) and two separate locations; central and 45° off the plane, in order to cover the full instrument workspace and account for different lesion sizes. In addition, two scaling factors for the translation component of the inverse kinematic control were compared using the small circle set-up. The big circle set-up was instead used to compare the performance of a wristed (7-DoF) and a non-wristed (6-DoF) tool. For each trial, each user was asked to repeat the task three times. An electromagnetic tracker (TrakSTAR, Ascension) was used to track the instrument tip position in 3D with the target being positioned directly on top of the field generator within 100mm for high accuracy. The corresponding value was recorded at each target, together with the overall task completion time. The experimental set-up is shown in Fig. 5.

The results of the user trials are reported in Fig. 6. The boxplots show the data distribution for each task among the five users. For each user, the task completion time was calculated as the average between the duration of the three trials. The desired target positions were found through a k-means algorithm as the centroids of the recorded tip position clusters over the three trials. The spatial deviation for each target was then calculated as the standard deviation of the three distances between the centroid and the recorded tip positions in the corresponding cluster.

The results clearly show comparable performance between users in terms of both positioning accuracy and execution time. The quality of performance is also consistent independently of lesion position or size, demonstrating the precision of instrument motion within the entire workspace. Sub-millimeter values of spatial deviation obtained for different scaling factors (Task 1 vs Task 2 and Task 3 vs Task 4) also show high positioning accuracy for both wrist and elbow components of the instruments. Wristed and non-wristed tools (Tasks 5 and 6 vs Tasks 7 and 8) show similar performance in terms of accuracy of targeting. However, the shorter completion time obtained for Tasks 7 and 8 suggests that control of the wristed tool is more intuitive.

2) Suture and wound closure

This trial aimed to test the overall performance of the system in its capability to undertake a surgical suturing task. The requirement for any system to perform a suturing task requires a complex interplay of dexterity, instrument interaction and force application within the arms and at the end-effectors to be reliable. This task consisted of passing a needle through a latex

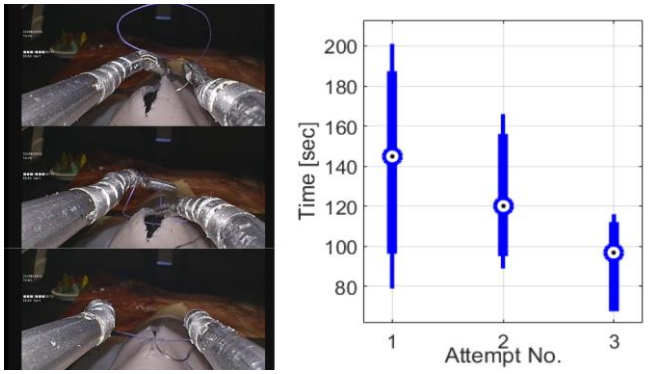

Fig. 7. Suturing on latex model; (left) snapshots during the study and (right) completion time for five engineers performing the task (3 trials).

This article has been accepted for publication in a future issue of this journal, but has not been fully edited. Content may change prior to final publication. Citation information: DOI 10.1109/LRA.2017.2668461, IEEE Robotics and Automation Letters

simulated wound model, two throws of the suture thread are looped on the left instrument and the other end is pulled through to make the initial throw of the surgical knot.

Five novices with engineering background performed the single knot-tying task. The users had different levels of familiarity with the robot, however no one had extensive training on the task. The users were asked to watch a video of the procedure and practice it once. Each user had then three attempts and the time to complete the task was recorded and shown in Fig.7. The average completion time was 142s, 120s, 98s for the three attempts respectively. For most users, the time to complete the task decreased at the second and third attempt.

B. Bovine Tissue Study

The study was carried out in a wet lab environment on bovine bowel tissue, which is considered an accurate representation of the human rectum. The experimental setup was arranged as in a real clinical scenario. Two separate trials were undertaken: a lesion marking and excision trial and subsequently the full procedure performed as would be representative of a true clinical case, including closure of the defect using a standard suture with a definitive three throw surgical knot.

For each of the trials the rectal tissue was tattooed with blue ink, each of uniform size (6mm) to represent a fixed lesion, standardised for each user. A 7-DoF grasper was mounted on the left side and a 4-DoF diathermy tool was mounted on the right side. The primary task was to mark the lesion with the electro-cautery tool, then excise it to full thickness depth. Fig. 8 shows different instances of the task.

Three clinicians with surgical backgrounds, performed the task after a standard brief introduction and familiarisation of the robot. One of the three clinicians performed the task 10 times to evaluate the early learning curve of the system. Time to complete the task was recorded and presented in Fig. 9 (left). In

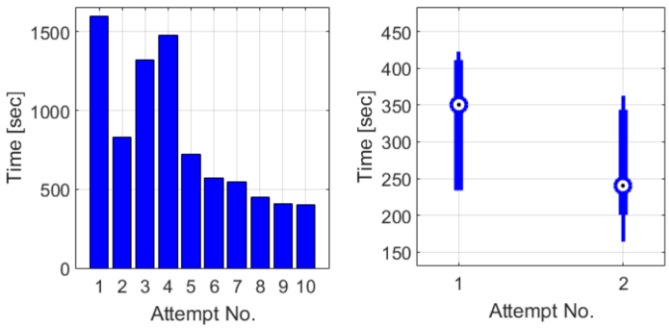

Fig. 9. Performance of full-thickness excision on bovine bowel; (left) completion time for 10 trials for one clinician performing the same task, and (right) completion time for five engineers for two trials.

all cases, the task was completed without difficulties. The results highlight that the time to complete the task reduced dramatically after familiarity with the robot was gained.

Furthermore, five users with engineering backgrounds performed the same task on the same tissue. Each user had two attempts. All the users had previous experience using the robot on other tasks, therefore there was no specific practice prior to the task. All five users completed the task without difficulties. The average time to finish the task was 330s in the first attempt, and 263s in the second attempt, see Fig. 9 (right). All five users took less time on the second attempt.

Two surgeons performed the suturing tasks on bovine bowel tissue. The purpose of this study was to test the capability of the robot on real clinical procedures. Both surgeons were able to perform closure with knot-tying. The closure was done with a needle with 9-10cm long thread and a bead applied at the end of the thread. Fig. 10 shows instances during the performance of a suturing and knot-tying task.

One of the surgeons performed six closures following the same steps, driving the needle four passes through the tissue

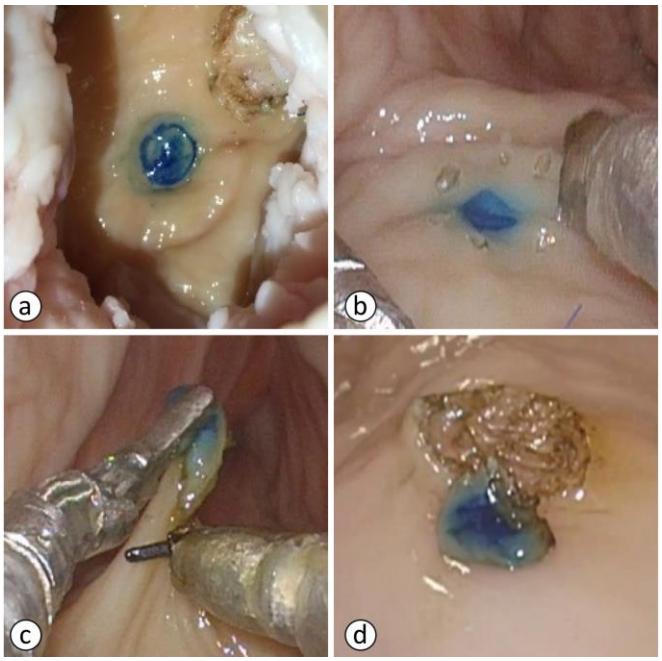

Fig. 8. Full-thickness excision on bovine bowel tissue: (a) simulated lesion, (b) marking, (c) excision and (d) excised tissue.

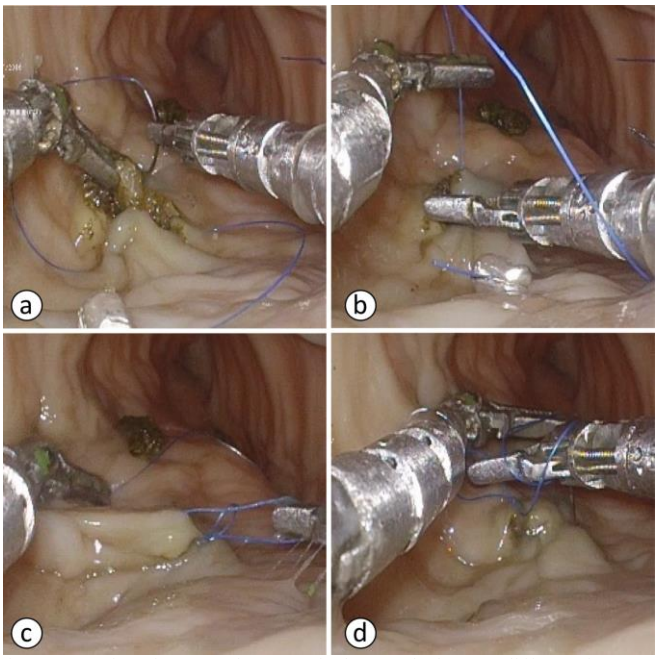

Fig. 10. Bovine tissue study – surgical wound closure; different instances during the performance of suturing and knot-tying.

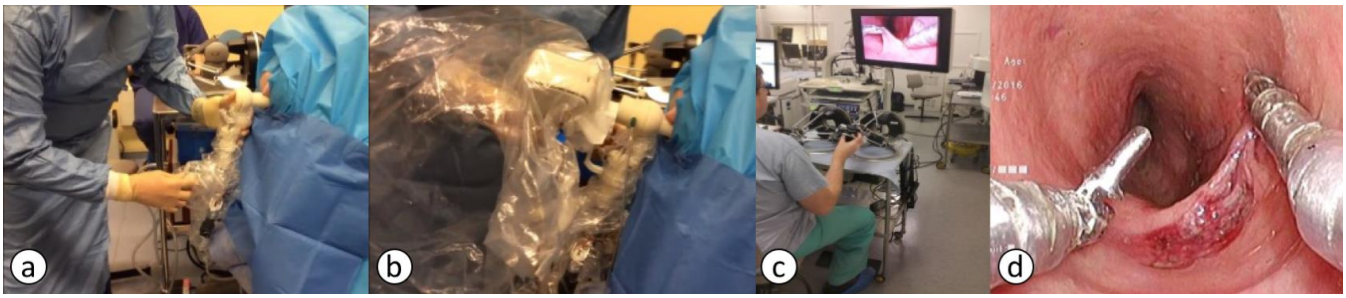

Fig. 11. *In-vivo* study on a porcine model: (a) support arm and port set up, (b) actuation pack attached, (c) surgeon in operation and (d) full-thickness dissection.

around the wound, followed by three knots to close the wound. The closure was completed in all six attempts.

C. In-Vivo Animal Trial

The *in-vivo* experiment was performed on a live porcine model under United Kingdom Home Office license number 70/7940 to the surgical workflow of a full TEMS procedure performed with the robot, from system setup to lesion removal and wound closure. Fig. 11 shows the system setup in operating theatre and being used on a porcine model.

The system setup requires fixing the support arm to the operating table and covering it with customised sterile cover; mounting the port onto the support arm before attaching the actuation packs to the port, then covering the actuation pack with another customised sterile cover; all now fully supported by the arm. The camera can then be inserted through the dedicated channel before inserting the instruments in readiness for the operation. The system setup took approximately 15 to 20min when performed by a licensed surgeon. Assistance was required only when mounting the support arm to the surgical bed.

The operation started with a diathermy instrument on the right hand and a grasper on the left hand to perform lesion marking and excision. Then, the diathermy tool was replaced by a needle driver instrument to perform the suturing task. The instrument exchange took less than 90s.

According to the feedback from the users that operated the robot, the two commercial products that we used in this system, the 3D camera (Olympus EndoEye Flex) and the omega.7 haptic devices, are not optimal for this purpose. The camera is too close to the instrument shafts, obstructing a large portion of the camera field of view. A custom camera that can provide off-axis view of the surgical site would provide better visualisation. Additional desired features include the addition of force sensors to measure forces applied to the instruments, and a new dedicated master device with haptic feedback and better ergonomic design to replace the general-purpose haptic devices.

V. CONCLUSIONS

In summary, this paper describes a single-port robotic surgical system designed for TEMS. The system comprises a master console and a slave robot platform. Design considerations of the robot platform and each of the components are described. Kinematic control of the surgical instruments is introduced. Extensive user study results show that the two instruments can be controlled precisely and the system is suitable for complex tasks in confined spaces. Full surgical procedures by clinicians were repeatedly carried out on bovine tissue and also in live animal trials, suggesting that the whole robotic system is effective and ergonomic for the operator in the proposed TEMS procedure.

REFERENCES

[1] M. Arnold, *et al.*, "Global patterns and trends in colorectal cancer incidence and mortality," *Gut,* pp. 0:1-9, 2016.

[2] L. Morelli, *et al.*, "Da Vinci single site© surgical platform in clinical practice: a systematic review," *The International Journal of Medical Robotics and Computer Assisted Surgery,* pp. 12(4):724-734, 2016 Dec, Epub 2015 Nov.

[3] J. H. Kaouk, *et al.*, "A Novel Robotic System for Single-port Urologic Surgery: First Clinical Investigation," *European Urology,* vol. 66, pp. 1033-1043, 2014.

[4] K. Roh, *et al.*, "Single-Port Surgical Robot System with Flexible Surgical Instruments," in *Intelligent Robotics and Applications*. vol. 9245, ed: Springer International Publishing, 2015, pp. 447-459.

[5] A. Bajo, *et al.*, "Integration and preliminary evaluation of an Insertable Robotic Effectors Platform for Single Port Access Surgery," in *IEEE International Conference on Robotics and Automation (ICRA)*, St. Paul, MN, USA, 2012, pp. 3381-3387.

[6] G. P. Haber, *et al.*, "SPIDER surgical system for urologic procedures with laparoendoscopic single-site surgery: from initial laboratory experience to first clinical application," *European Urology,* vol. 61, pp. 415-22, 2012.

[7] D. Giannotti, *et al.*, "Spider surgical system versus multiport laparoscopic surgery: performance comparison on a surgical simulator," *BMC Surgery,* vol. 15, p. 54, 2015.

[8] Y. Kobayashi, *et al.*, "Development of a robotic system with six-degrees-of-freedom robotic tool manipulators for single-port surgery," *International Journal of Medical Robotics,* vol. 11, pp. 235-46, Jun 2015.

[9] J. Shang, *et al.*, "Design of a Multitasking Robotic Platform with Flexible Arms and Articulated Head for Minimally Invasive Surgery," in *IEEE/RSJ International Conference on Intelligent Robots and Systems (IROS)*, Vilamoura, Portugal, 2012, pp. 1988-1993.

[10] V. Vitiello, *et al.*, "Emerging robotic platforms for minimally invasive surgery," *IEEE Reviews in Biomedical Engineering,* vol. 6, pp. 111-26, 2013.

[11] H. W. Zhang, *et al.*, "Torque Estimation for Robotic Joint With Harmonic Drive Transmission Based on Position Measurements," *IEEE Transactions on Robotics,* vol. 31, pp. 322-330, 2015.

[12] C. A. Seneci, *et al.*, "Rapid Manufacturing with Selective Laser Melting for Robotic Surgical Tools: Design and Process Considerations," *IEEE/RSJ International Conference on Intelligent Robots and Systems (IROS),* pp. 824-830, 2015.

[13] S. Papagrigoriadis, "Transanal endoscopic micro-surgery (TEMS) for the management of large or sessile rectal adenomas: a review of the technique and indications," *International Seminars in Surgical Oncology,* vol. 3, p. 13, 2006.

[14] K. Leibrandt, *et al.*, "Effective Manipulation in Confined Spaces of Highly Articulated Robotic Instruments for Single Access Surgery," *IEEE Robotics and Automation Letters,* 2017, In press.